

Accepted Manuscript

Promoting *in vivo* early angiogenesis with sub-micrometer strontium-contained bioactive microspheres through modulating macrophage phenotypes

Fujian Zhao, Bo Lei, Xian Li, Yunfei Mo, Renxian Wang, Dafu Chen, Xiaofeng Chen



PII: S0142-9612(18)30424-1

DOI: [10.1016/j.biomaterials.2018.06.004](https://doi.org/10.1016/j.biomaterials.2018.06.004)

Reference: JBMT 18705

To appear in: *Biomaterials*

Received Date: 11 April 2018

Revised Date: 28 May 2018

Accepted Date: 5 June 2018

Please cite this article as: Zhao F, Lei B, Li X, Mo Y, Wang R, Chen D, Chen X, Promoting *in vivo* early angiogenesis with sub-micrometer strontium-contained bioactive microspheres through modulating macrophage phenotypes, *Biomaterials* (2018), doi: 10.1016/j.biomaterials.2018.06.004.

This is a PDF file of an unedited manuscript that has been accepted for publication. As a service to our customers we are providing this early version of the manuscript. The manuscript will undergo copyediting, typesetting, and review of the resulting proof before it is published in its final form. Please note that during the production process errors may be discovered which could affect the content, and all legal disclaimers that apply to the journal pertain.

**Promoting *in Vivo* Early Angiogenesis with Sub-micrometer Strontium-contained Bioactive
Microspheres through Modulating Macrophage Phenotypes**

Fujian Zhao ^{a, c, d}, Bo Lei ^{b, e, f *}, Xian Li ^{a, c, d}, Yunfei Mo ^{a, c, d}, Renxian Wang ^g, Dafu Chen ^{g *}, Xiaofeng
Chen ^{a, c, d *}

^a *Department of Biomedical Engineering, School of Materials Science and Engineering, South China
University of Technology, Guangzhou 510641, China*

^b *Frontier Institute of Science and Technology, Xi'an Jiaotong University, Xi'an 710000, China*

^c *National Engineering Research Center for Tissue Restoration and Reconstruction, Guangzhou 510006,
China*

^d *Key Laboratory of Biomedical Materials and Engineering, Ministry of Education, South China University
of Technology, Guangzhou 510006, China*

^e *Instrument Analysis Center, Xi'an Jiaotong University, Xi'an 710054, China*

^f *State Key Laboratory for Manufacturing Systems Engineering, Xi'an Jiaotong University, Xi'an 710054,
China*

^g *Laboratory of Bone Tissue Engineering, Beijing Laboratory of Biomedical Materials, Beijing Research
Institute of Orthopaedics and Traumatology, Beijing Jishuitan Hospital, Beijing, 100035, China*

**Corresponding authors:*

E-mail: rayboo@xjtu.edu.cn (Bo Lei),

E-mail: chendafu@jsthospital.org (Dafu Chen),

Email: chenxf@scut.edu.cn (Xiaofeng Chen)

Abstract: Early vascularization capacity of biomaterials plays an essential role in efficient wound healing and tissue regeneration, especially in large tissue tension implanting position such as bone augmentation. Strontium-contained silica-based bioactive materials have shown the role of promoting angiogenesis by stimulating osteoblasts to secrete angiogenesis related cytokines. However, osteoblasts have little effect on early angiogenesis due to the inflammatory reaction of implantation site. Here, for the first time, we found that the monodispersed strontium-contained bioactive glasses microspheres (SrBGM) could significantly promote the early angiogenesis through regulating macrophage phenotypes. After being stimulated with SrBGM *in vitro*, RAW cells (macrophages) presented a trend towards to M2 phenotype and expressed high level of platelet-derived growth factor-BB (PDGF-BB). Moreover, the RAW conditioned medium of SrBGM significantly enhanced the angiogenic capacity of HUVECs. The *in vivo* early vascularization studies showed that significant new vessels were observed at the center of SrBGM-based scaffolds after implantation for 1 week in a bone defect model of rats, suggesting their enhanced early vascularization. Due to the efficient vascularization, the *in vivo* new bone formation was promoted significantly. Our study may provide a novel strategy to promote the early vascularization of biomaterials through modulating the microphage phenotypes, which has wide applications in various tissue regeneration and wound healing.

Keywords Strontium; Bioactive glasses; Micro-nano Particles; Angiogenesis; Macrophage phenotypes; Bone regeneration

1. Introduction

Native tissue regeneration greatly depends on the vascular networks which provide the essential nutrients and oxygen. Therefore, it is very crucial for biomaterials to restore a vascular network to support the cell survival and new tissue formation. Especially, during the reconstruction of atrophic alveolar ridge,

the bone augmentation is usually necessary. Unlike the filling bone defect cavity, the bone augmentation needs to increase the space for implantation which will increase the tissue tension and cause the surrounding tissue to be in an ischemic state.[1] The long time ischemia will lead to the failure of the operation with the exposure of implants. So, the angiogenesis at the implantation site is crucial for the success of bone augmentation in the early stage.

In recent years, bioactive glasses (BGs) have drawn much attention due to its attractive osteoconductive and osteoinductive properties.[2, 3] They have been widely used in repairing bone defects caused by infection, trauma and tumor, as well bone augmentation in atrophic alveolar ridge.[4, 5] In previous studies, some inorganic ions have incorporated into BGs to improve their osteogenesis and angiogenesis properties, such as strontium (Sr), cobalt (Co), lithium (Li), copper (Cu), europium (Eu) and zirconium (Zr) [6-9]. Among these bioactive elements, Sr has aroused great attention since it has been reported to stimulate bone formation and decrease bone resorption [10-12]. *In vitro* studies indicated that Sr ions could enhance the proliferation and differentiation of osteoprogenitor cells into bone-forming osteoblasts by activating membrane-bound calcium sensing receptor (CaSR) and Wnt/ β -catenin signaling pathway [13, 14]. Clinically, strontium ranelate (Sr RAN) has been used for post-menopausal osteoporosis by significantly increasing bone strength [15]. Moreover, Sr is also reported to have the function of promoting angiogenesis.[16] For example, the release of Sr ions in tissue-engineered bone could stimulate the expression of proangiogenic factors such as vascular endothelial growth factor (VEGF), basic fibroblast growth factor (bFGF) and matrix metalloproteinase-2 (MMP-2) [17]. However, most of the literatures report that Sr ions enhance the angiogenesis by promoting osteoblasts to secrete vascular related cytokines.[18-21] It should be realized that when the materials are implanted, an acute inflammatory

reaction will happen and osteogenesis occurs after the foreign body response.[22] So, the osteoblasts have little effect on the angiogenesis of biomaterials at the early stage of implantation. It is not clear if BGs could enhance the angiogenesis through other biological pathways such as the regulation of inflammatory cell state.

During the inflammatory reaction stage, monocyte/macrophage system is the major regulator of inflammatory response.[23] Upon surgical implantation, monocytes are rapidly recruited to the injury site and differentiate into macrophages. The regulation effects are mainly through their unique plasticity which can rapidly shift their phenotype in response to the environmental stimuli. Generally, macrophages are divided into two phenotypes, known as the M1 (pro-inflammatory) polarization and M2 (anti-inflammatory) polarization.[24] M1 macrophages are responsible for recruiting inflammatory cells to the site of injury and for instigating the foreign body response. Oppositely, M2 macrophages are believed to promote tissue deposition and remodeling.[25, 26] Macrophages are known to play an importance role in vascularization by producing several potent angiogenic factors including vascular endothelial growth factor (VEGF), basic fibroblast growth factor (bFGF) and transforming growth factor- β (TGF- β).[27, 28] Although the roles of different macrophage phenotypes in angiogenesis are currently controversial, M2 macrophages are typically described as the angiogenic phenotype.[29-31] During the tissue repair process, M1 macrophages dominate at early times (1-5 days) after injury, while M2 macrophages control the later stages (7-14 days).[32, 33] Therefore, it is a feasible way of regulating the immune response for improved angiogenesis through regulating the macrophage phenotype.[34]

Recent studies have indicated that harnessing the inflammatory response can be an effective strategy for improving tissue healing and regeneration.[35] Our previous study also demonstrates that

strontium-substituted bioactive glass (SrBG) has the ability to promote osteogenesis by inhibiting the inflammatory response of macrophage.[36] However, to date, the effect of SrBG on angiogenesis by regulating macrophage phenotype remains unclear. Therefore, in this study, for the first time, we investigate the effect of Sr-substituted BG microsphere (SrBGM) on the macrophage phenotype, angiogenesis under the inflammatory state and bone augmentation *in vitro* and *in vivo*.

2. Materials and methods

2.1. Synthesis and characterization of BGM and SrBGM

The synthesis and characterizations of monodispersed BGM and SrBGM was performed according to our previous report.[36, 37] The molar composition of BGM and SrBGM were $60\text{SiO}_2\text{36CaO4P}_2\text{O}_5$ and $60\text{SiO}_2\text{26CaO10SrO4P}_2\text{O}_5$, respectively. In brief, a given amount of dodecylamine (DDA) was dissolved in 25 ml deionized water and 80 ml Ethanol. Then, 16 mL tetraethyl orthosilicate (TEOS, Guanghai Chemical) were added to the above solutions and stirred for 1h. After that, triethylphosphate (TEP, Aladdin) and calcium nitrate tetrahydrate (CN, Guanghai Chemical) or strontium nitrate (SN, Guanghai Chemical) were added in order in the proportions at 30 minute intervals while magnetically stirring at 40 °C. The resulted solution was vigorously stirred together for another 3 h, and the white precipitates were collected by filtration and dried at 60 °C for 24 h. BGM and SrBGM were obtained after removing templates and organic components by calcifying under air atmosphere at 650 °C for 3 h. The morphology and structure of the microspheres was characterized by scanning electron microscopy (SEM, DSM 982-Gemini, Zeiss, Germany), Fourier Transform Infrared Spectrometry (FTIR, VERTEX 33 Bruker, Germany), X-ray diffraction (XRD, X'pert PRO, Panalytical, Netherlands) and multipoint Brumauer-Emmett-Teller (BET) N_2 absorption technique (NOVA4200e, Quantachrome).

2.2 Fabrication and characterization of gelatin/bioactive glass scaffolds

In order to investigate the effect of SrBGM on the *in vivo* angiogenesis and bone formation, gelatin/BGM (Gel-BGM) and gelatin/SrBGM (Gel-SrBGM) scaffolds were fabricated by a freeze drying method. In brief, 2.8 g BGM or SrBGM and 1.2 g gelatin were dispersed in 20 mL deionized water and stirred for 4 h at 40 °C. After that, the suspensions were directly mixed with 3 mL genipin solution (1 wt%). After vigorous stirring for 20 min, the suspensions were freeze-dried at -20 °C for 12 h and freeze-dried, for 24 h. In addition, the gelatin scaffolds (Gel) without adding bioactive glass were prepared by the same method and used as control group. The surface morphology and porous structure of the composite scaffolds was characterized by SEM and Micro-CT (ZKKS-MCT-SharpII, Zhongke Co., China) operated at a voltage of 60 kV and an electric current of 67 mA.

2.3 Cell culture

The murine-derived macrophage cell line RAW 264.7 cells (RAW) and human umbilical vein endothelial cells (HUVECs) were used in *in vitro* study. RAW were obtained from Chinese Academy of Sciences and incubated in Dulbecco's Modified Eagle Medium (DMEM, Life Technologies, Carlsbad, California, USA) supplemented with 10% fetal bovine serum (FBS, Thermo Scientific, Waltham, Massachusetts, USA) and 1% (v/v) penicillin/streptomycin (P/S, Life Technologies, Carlsbad, California, USA). HUVECs were purchased from the American Type Culture Collection (ATCC) and cultured in endothelial cell medium (ECM, ScienCell, USA) with 5% FBS and 1% endothelial cell growth supplement/heparin kit (ECGS/H, Promocell). All the cells were incubated at 37 °C in an atmosphere with 95 % humidity and 5% CO₂. After the confluence reach to 90%, cells were passaged using 0.25% trypsin with EDTA. The third to eight passages cells were used in this study. BGM and SrBGM extracts were

prepared for testing *in vitro* angiogenesis property. Briefly, sterilized BGM and SrBGM powders were added into DMEM or ECM medium at a ratio of 1 mg/mL and then maintained at 37 °C with a shaking speed of 120 rpm for 24 h. After that, the materials extracts were obtained by centrifugation and filtration. The concentrations of Si, Ca, P and Sr ions were analyzed by inductively coupled plasma atomic emission spectrometer (ICP-AES, Varian 720). Before cells culture, the BGM and SrBGM extracts were diluted by normal culture medium in a ratio of 1:3. In addition, the normal growth medium and normal growth medium containing 10 μ M SrCl₂ were used as control groups, which were marked as Control and SrCl₂ group.

2.4 Angiogenesis properties evaluation

The angiogenesis effect was evaluated by immunofluorescent staining of CD31 and mRNA expressions of angiogenesis-related genes. Briefly, HUVECs were seeded at a density of 3000 cells per well in 96-well plates. After attachment for 24 h, the cell media were replaced by Control, SrCl₂, BGM and SrBGM extracts, respectively. After cultured for 3 days, the cells were fixed in 4% paraformaldehyde for 30 min and washed with phosphate-buffered saline (PBS). Then the cells were permeabilized with 0.5 % Triton X-100 for 10 min followed by PBS wash. After that, the cells were blocked in bovine serum albumin (BSA) for 1 h at room temperature (RT), and incubated with primary antibody of CD31 (1:80 dilution; Thermo Fisher, China) overnight at 4 °C. After being rinsed with PBS for 3 times, cells were incubated with Cy3-conjugated goat anti-mouse immunoglobulin G (1:200 dilution; Invitrogen, USA) for 1 h. Finally, cell nuclei were stained with DAPI (Beyotime). Images were captured by an inverted fluorescence microscope (Eclips Ti-U, Nikon, Japan). The fluorescence intensity was calculated using Image J software.

To examine angiogenesis-related genes expressions, HUVECs with a seeding density of 1×10^5

cells/well were plated in 24-well plates. After 24 h, the culture medium was replaced by Control, SrCl₂, BGM and SrBGM extracts, respectively. After cultured for 3 days, the genes expressions of Angiogenin, FGF-2 and SDF were analyzed by real-time quantitative polymerase chain reaction (RT-qPCR). Typically, total RNA was extracted using HiPure Total RNA Micro Kit (Magen) following the manufacturer's instructions. The isolated RNA was then reverse transcribed into cDNA by using the Reverse Transcription Reagents Kit (Takara). The RT-qPCR was performed by using a Maxima SYBR Green/ROX qPCR (Thermo Scientific) and conducted on a Quantstudio 6 Flex (Life technologies). The gene expressions were calculated by the $2^{-\Delta\Delta C_t}$ method. The sequences of primers for Angiogenin, FGF-2 and SDF genes were given in Table S1. The relative expression of the genes of interest was normalized against the housekeeping gene GAPDH.

2.5 Macrophage phenotypes regulation assessment

RAW cells were seeded in 6-well plates at a density of 1.5×10^5 cells/well. After cultured for 12 h, the cells were treated with lipopolysaccharide (LPS, Beyotime) at a concentration of 100 ng/mL for 8 h to polarize M0 macrophages into M1 phenotypes. After rinsed in PBS for 3 times, the cells medium were replaced by Control, SrCl₂, BGM and SrBGM extracts for 3 days. The conditioned medium was obtained by mixing the RAW-cultured medium with the ECM complete medium at a ratio of 1:1 (denoted as Control+RAW, SrCl₂+RAW, BGM+RAW and SrBGM+RAW). The images of LPS treated cells were captured by inverted fluorescence microscope. Prior to observation, samples were fixed in 4% paraformaldehyde and stained with fluorescein isothiocyanate (FITC)-phalloidin (Sigma) and DAPI.

The expression of M1 and M2 surface markers of RAW after cultured for 3 days with the four groups mediums were determined by flow cytometry. Briefly, the cells were scraped off and centrifuged at 1000 rpm for 5 min. After resuspension and blocking with 1% BSA/PBS, cells were incubated with CD11c antibody

(M1 marker, 1:400 dilution, Thermo Fisher) and CD206 antibody (M2 marker, 1:300 dilution, Thermo Fisher) on ice. After 30 min, the cells suspension solution was performed on a Guava EasyCyte HT system (Merk Millipore). The results were analyzed by Guava Soft 2.5. The macrophage polarization (TNF α , IL1 β , IL6, IL10, IL1ra and Arginase), osteogenesis (BMP2), fibrosis (TGF β 1, TGF β 3) and angiogenesis (VEGF and PDGF-BB) related gene expressions were detected by RT-qPCR. The experimental procedure was described in section 2.4, and the results were normalized to the expression of house-keeping gene GAPDH. The primer sequences and genes studied in this section are presented in Table S2.

Western blotting analysis was performed for the detection of the PDGF-BB protein expression after 3 days of culture. The cell lysates were obtained by lysing the cells in RIPA buffer (Beyotime). Proteins (10 mg) separation was performed on SDS-PAGE gels, which were subsequently transferred onto a PVDF membrane. After being blocked with 5% non-fat dried milk, the membranes were incubated with primary antibodies against, including PDGF-BB (1:1000, Abcam, AB53716, UK) and β -actin (1:3000, Servicebio, GB12001, China) overnight at 4 °C. The membranes were washed three times in Tris-buffered saline supplemented with 0.05% Tween 20 (TBST), and then incubated with anti-mouse/rabbit HRP conjugated secondary antibodies at 1:2000 dilutions for 1 h at room temperature. The protein bands were visualized using the SuperSignal West Femto Maximum Sensitivity Substrate and exposed on X-ray films (Fujifilm, Australia). Quantitative densitometric analysis was carried out using Image J software.

2.6 Angiogenesis properties of HUVECs in RAW conditioned medium

The angiogenesis effect of the RAW conditioned medium (Control+RAW, SrCl₂+RAW, BGM+RAW and SrBGM+RAW) obtain from section 2.5 were evaluated by immunofluorescent staining of CD31 and mRNA expressions of angiogenesis-related genes (Angiogenin, FGF-2 and SDF). The experimental

procedure was described as section 2.4.

2.7 *In vivo* angiogenesis and bone regeneration evaluation

2.7.1 Surgical procedure and treatment

Twelve Balb/c mice (male, 25~30 g) and twenty four sprague-dawley rats (SD rats, male, 200~250 g) were purchased from Laboratory Animal Center, Southern Medical University. All animal procedures were performed following protocol approved by the Institutional Animal Care (Guangdong Pharmaceutical University). A subcutaneous implants experiment was used to investigate the inflammatory reaction of Gel-SrBGM. All the Balb/c mice were equally divided into three groups (Gel, Gel-BGM and Gel-SrBGM). The mice were anesthetized using 10% chloral hydrate. An incision of 1 cm at left side of back was made and a subcutaneous pocket was created. Then one scaffold was embedded subcutaneously. Three days later, all mice were euthanized. The implanted substances were dissected from the mice. All harvested samples were lysed by RIPA lysis buffer (Beyotime) for ELISA detection of IL6 (RayBiotech, USA) and IL1 β (RayBiotech, USA).

The SD rats were used to evaluate angiogenesis and bone regeneration properties. The bone augmentation animal model was adapted from previous study.[38] After general anesthesia by 10 % chloral hydrate, the rats were shaved the hair at head and disinfected with iodine. A sagittal incision of approximately 15 mm was made on the scalp, and the calvarium was exposed by blunt dissection. One scaffold with a diameter of 6 mm and thickness of 2 mm was inserted subcutaneously, which was then closed with the silk 3-0 suture. After feeding for 1 and 6 weeks, 4 rats of each group were sacrificed using an overdose of sodium pentobarbital. The scaffolds together with surrounding skull were cut off and fixed in 10% of phosphate-buffered formalin for 5 days before further analysis.

2.7.2 Micro-CT analysis and histological evaluation

The Micro-CT (ZKKS-MCT-SharpII, Zhongke Co., China) analysis was operated at a voltage of 60 kV and an electric current of 67 mA. The voxel size after reconstruction was $25 \times 25 \times 25 \mu\text{m}$. Based on the Micro-CT results, three-dimensional images were reconstructed by MIMICS (Materialise's interactive medical image control system, Materialise Co., Belgium). The bone volume to total bone volume (BV/TV) of 6 weeks groups was determined using the analysis software.

Following Micro-CT scan, the samples were decalcified in 10% EDTA for 4 weeks and then embedded in paraffin parallel to the sectioned surface. Serial cross-sections of decalcified samples were sectioned for hematoxylin and eosin (H&E) and Masson's trichrome staining according to the manufacturer's instructions. In addition, the samples at 1 week were stained with immunohistochemistry of M1 marker inducible nitric oxide synthases (NOS2, Santa Cruz Biotechnology), M2 markers CD206 (Santa Cruz Biotechnology) and Arginase I (Santa Cruz Biotechnology). The samples at 6 week were stained with OCN (1:200, Servicebio, GB11233, China) and BMP2 (1:500, Servicebio, GB11252, China). Then images were acquired using a microscope (Axioskop 40 FL, Zeiss) and a video camera (Soft Imaging System).

2.8 Statistical analysis

The data were presented as mean \pm standard deviation. One-way analysis of variance (ANOVA) was used to analyze the significant differences between samples. A value of $p < 0.05$ was considered statistically significant.

3. Results

3.1 Physicochemical structure characterization of SrBGM and SrBGM-based scaffolds

BGM and SrBGM were prepared by the combination of sol-gel method and template self-assembly

technique. SEM and EDS results indicated that the Sr was successfully incorporated into BG microspheres and the microspheres still maintained uniform particle sizes with the diameter approximately 400-500 nm, which was similar to BGM (Fig. 1A). XRD (Fig. 1B) and FTIR (Fig. 1C) results confirmed that the SrBGM still showed the representative amorphous structure and Si-O-Si composition. The specific surface area, pore volume, mean pore size of samples was 12.74 m²/g, 0.10 cm³/g, 3.4 nm for BGM and 10.37 m²/g, 0.047 cm³/g, 4.3 nm for SrBGM, respectively. In order to maintain a stable porous structure for *in vivo* implantation, freeze-drying method was used to prepare composite scaffolds by mixing SrBGM with gelatin. The morphology and structure of the scaffolds were shown in Fig. 1D. Micro-CT results confirmed that scaffolds presented a porous structure (insert images in Fig. 1D), and the SEM results clearly indicated that all of the scaffolds presented highly interconnected porous structure with a mean pore size of 200-800 μm. Enlarged images clearly indicated that Gel-BGM and Gel-SrBGM were consisted of uniform, dispersed and spherical BG nanoparticles, while the Gel just showed the smooth surface of gelatin.

3.2 *In vitro* angiogenesis of HUVECs

The BGM and SrBGM extracts were used to evaluate *in vitro* angiogenesis and the ions concentration were shown in Table S3. The Si, Ca and P ions concentration were similar between BGM and SrBGM. The concentration of Sr ion in SrBGM extracts was 6.227 mg/L. The effect of Sr adding in BGM on the *in vitro* angiogenesis of HUVECs was shown in Fig. 2. Immunofluorescence assay demonstrated that a large amount of CD31 positive staining in BGM and SrBGM could be observed compared to Control group, indicating that BGM and SrBGM expressed higher levels of CD31 (Fig. 2A). Quantitative analysis of immunofluorescence intensity further verified the result that the CD31 intensity of BGM and SrBGM were significantly higher than Control group, while the SrCl₂ had no significant difference in comparison

with Control group ($p < 0.05$) (Fig. 2B). In addition, immunofluorescence intensity of CD31 between BGM and SrBGM had no significant difference. The angiogenesis-related genes expression presented a similar trend with immunostaining (Fig. 2C). The expression level of FGF-2 and SDF were significantly upregulated after treatment of BGM and SrBGM than the Control group, and gene expression of SrCl₂ had no obvious change ($p < 0.05$). These results suggested that both BGM and SrBGM enhanced the angiogenesis of HUVECs *in vitro*, and the addition of Sr into BGM had no significant difference effect.

3.3 Macrophage polarization regulation and angiogenesis potential

Due to the inflammatory state at early implantation, it encouraged us to investigate the effect of SrBGM on the macrophage polarization and angiogenesis. In order to mimic the *in vivo* acute inflammatory state, LPS was used to induce RAW to M1 phenotype. After 8 h of treatment, some pseudopodia could be observed indicating that RAW had a tendency to polarizing to M1 (Fig. S1). After incubated with Control, BGM, SrBGM and SrCl₂ for 3 days, the flow cytometry results showed that in comparison with Control group, the M1 marker CD11c expression in other groups was reduced (Fig. 3A). However, there were more RAW cells expressing M2 marker CD206 after treated by SrBGM and SrCl₂, as compared to BGM (Fig. 3A). Consistently, the expression of pro-inflammatory gene TNF, IL1 β and IL6 in SrBGM and SrCl₂ groups were significantly downregulated in comparison with the Control group (Fig. 3B). As for the anti-inflammatory genes, the expression IL10 and Arginase in BGM, SrBGM and SrCl₂ were significantly upregulated compared with Control group. However, we also observed that the SrBGM group showed the significantly high expression of IL10 and Arginase, as compared to BGM group ($p < 0.05$). These results demonstrated that after stimulated with SrBGM for 3 days, the RAW presented a trend towards to M2 phenotype.

The effect of SrBGM on the angiogenesis of macrophage was also studied by RT-qPCR and western blot analysis. The VEGF gene expression of SrBGM and SrCl₂ had no significantly difference in comparison with BGM (Fig. 3C). However, the mRNA expressions of PDGF-BB in SrBGM presented significantly higher level than BGM ($p < 0.05$). In addition, the relative protein expression of PDGF-BB in the SrBGM and SrCl₂ groups were significantly higher than BGM group (Fig. 3D and E), which was consistent with mRNA expressions results. These results indicated that SrBGM could significantly enhance the *in vitro* angiogenesis of macrophage. The fibrogenic and osteogenesis related gene expressions were also tested, as macrophages could release cytokines to participate in osteogenesis and fibrosis [39, 40]. Compared with BGM, the SrBGM group significantly increased the expression of osteogenesis related gene BMP2, indicating the incorporation of Sr into BGM could improve osteogenesis ($p < 0.05$) (Fig. S2). However, the fibrous related gene (TGFβ1, TGFβ3) expression had no significant difference between the four groups ($p > 0.05$).

3.4 Effects of RAW conditioned medium on angiogenesis of HUVECs

To further study the role of macrophage regulation in angiogenesis, the effect of SrBGM stimulated RAW cells on the angiogenic capacity of HUVECs was investigated (Fig. 4). After incubation 3 days, significantly high CD31 immunofluorescence positive staining was observed for SrBGM+RAW group, as compared to Control+RAW, BGM+RAW, SrCl₂+RAW groups (Figs. 4A-B). Moreover, some circles surrounded by CD31 positive proteins could be observed in SrBGM+RAW (yellow arrows) indicating the formation of relatively mature vascular lumina in HUVECs. The angiogenesis-related genes expression presented a similar trend with immunofluorescence analysis (Fig. 4C). The expression level of Angiogenin and SDF were significantly upregulated after treatment of SrBGM+RAW and SrCl₂ conditioned medium

compared with BGM+RAW group ($p < 0.05$). These data demonstrated that SrBGM regulated macrophage could significantly enhance the angiogenesis *in vitro* of HUVECs.

3.5 *In vivo* angiogenesis at early stage of implantation

The *in vivo* angiogenesis at early stage of implantation (1 week) was evaluated by implanting Gel, Gel-BGM and Gel-SrBGM in a bone augmentation model of rat. The gross observation and Micro-CT results confirmed that all scaffolds still maintained their original shape (Fig. 5A, B). Moreover, the scaffolds were wrapped in a layer of fibrous connective tissue film from the digital photo (Fig. 5A). However, the tissue thickness in Gel-BGM and Gel-SrBGM was significantly thicker than Gel from H&E (Fig. 5C). We further observed the center area of the scaffolds to evaluate angiogenesis condition (yellow box in first column of Fig. 5C). It was interesting that the cells could only be observed in the Gel-SrBGM group and some cells had formed vascular-like structures (yellow arrows). Immunohistochemical staining confirmed that a large number of CD31 positive proteins could be observed in the center area of Gel-SrBGM, indicating the formation of new blood vessels (Fig. 5D).

The inflammatory reaction at early stage of implantation was further studied. Subcutaneous implants experiment indicated that the pro-inflammatory cytokines (IL6 and IL1 β) expression of Gel-SrBGM were significantly downregulated compared with Gel-BGM at 3 days (Fig. S3). Moreover, the *in vivo* macrophage polarization on the edge of the scaffolds in bone augmentation model of rat at 1 week was studied, as shown in Fig.6. The M1 phenotype marker (NOS2) and M2 phenotype markers (CD206 and Arginase I) were detected. At 1 week, more NOS2 (M1) positive stained areas were found in Gel and Gel-BGM, compared with Gel-SrBGM. However, the M2 markers of CD206 and Arginase I presented an opposite trend. The CD206 and Arginase I (M2) positive areas of Gel-SrBGM were significantly more than

Gel-BGM, which indicated most of the macrophages had polarized to M2 at 1 week.

3.6 *In vivo* bone regeneration evaluation

The ultimate purpose of early angiogenesis of biomaterials is to enhance their tissue regeneration capacity. Therefore, we further studied the osteogenic potential of Gel, Gel-BGM and Gel-SrBGM scaffolds for 6 weeks. All the scaffolds had closely attached to the skull surface without any space (Figs. 7A-B). Quantitative analysis indicated that the value of the BV/TV in Gel-SrBGM group was statistically higher than Gel-BGM at 6 weeks ($p < 0.05$) (Fig. 7C). New bone formation was further evaluated by the histological analysis as shown in Fig. 7D and Fig. S4. The general view of Masson's trichrome and H&E staining indicated that Gel-BGM and Gel-SrBGM scaffolds had completely combined with the skull, which was consistent with Micro-CT results. In addition, both Gel-BGM and Gel-SrBGM had been filled with fibrous tissue, while most of Gel had been degraded. The enlarged image of Gel-SrBGM clearly presented that most of the residual scaffolds had been replaced by new bone islands. Some cuboid osteoblasts could be observed at the edge of the scaffold (yellow arrows in Fig. 7D), which indicated the formation of active osteogenesis. However, the new bone area of Gel-BGM was less than Gel-SrBGM. Immunohistochemical staining of osteogenic related proteins BMP2 and OCN also confirmed that positive stained areas of Gel-SrBGM were much more than Gel-BGM (Fig. S5).

4. Discussion

The promoting angiogenesis of implanted biomaterials at early stage could significantly enhance the new tissue regeneration. However, the early inflammatory reaction usually prevented the angiogenesis process of osteoblasts and epithelial cells.[41] In this study, we explored the effect of Sr in SrBGM on the angiogenesis and bone augmentation of inflammation-related macrophage *in vitro* and *in vivo*. SrBGM has

no significant effect on regulating the angiogenesis of HUVECs comparing with BGM. However, SrBGM could significantly enhance the M2 phenotype transformation and angiogenic genes expression of macrophage. *In vivo* experiments confirmed that SrBGM significantly promoted the vascularization formation and new bone regeneration.

In previous reports, silicon released from bioactive glass has been shown to stimulate angiogenesis by secretion pro-angiogenic cytokines.[42, 43] Moreover, some modification strategies for BG scaffolds have been developed to further promote angiogenesis, including the addition of inorganic ionic components, growth factors and drugs, manipulation of angiogenic growth factors and mimicking hypoxic conditions.[44] Our experiments also show that BG has the role to stimulating angiogenesis. However, the adding Sr has no extra effects of stimulating angiogenesis. Although Sr ions has been reported to have the effect of promoting angiogenesis by stimulating the expression of proangiogenic factors in tissue-engineered bone[45], no significant differences are found between BGM and SrBGM in our experiments. This result was different with previous reports in which the interaction of multiple ions such as Sr-Co [46] and Sr-Cu [47] enhanced the angiogenesis.

It is widely accepted that Sr has the effect to inhibit the secretion of proinflammatory cytokines, such as TNF- α and IL-6.[48, 49] However, *in vitro* experimental designs, the different Sr ions concentration will result in different macrophages polarization effects. For example, the high Sr ions concentrations (around 500 $\mu\text{mol L}^{-1}$) will inhibit the release of IL6 [50], while at a low Sr ions concentration (10 $\mu\text{mol L}^{-1}$) the inhibition effect is not obvious [48]. Our results also confirmed that more M2 macrophage can be observed both in SrBGM and SrCl₂ groups at foreign body response stage. However, the ability to improve M2 polarization of SrBGM is stronger than SrCl₂ based on the flow cytometry and mRNA expression results.

As the two groups have similar concentration of Sr ions, the difference is mainly attributed to the ions released from bioactive glass. A previous study has reported that BG ionic products could activate macrophages towards M2 phenotype and stimulate macrophages to express more anti-inflammatory cytokines. [51] Therefore, the Sr ions and other ions (Si, Ca and P) released from SrBGM could synergistically promote macrophages polarization to M2 phenotype.

We further explore angiogenesis with the effect of macrophage phenotypes transformation. In fact, the roles of different macrophage phenotypes in angiogenesis have been widely investigated. Traditionally, M2 macrophages are described as the angiogenic phenotype while M1 macrophages have little effect on angiogenesis.[30, 52] However, a recent report by Spiller *et al.* suggests that both M1 and M2 macrophages are necessary for enhanced vascularization and they contribute to angiogenesis in different ways.[53, 54] M1 macrophages expressed and secreted factors that promote the initiation of angiogenesis, especially VEGF. M2 macrophages secreted factors involved in later stages of angiogenesis, especially PDGF-BB, which functions as stabilizing the formation of the vasculature.[33, 53] In addition, PDGF-BB has the functions of promoting pericytes wrap around the blood vessels and preventing them from regressing.[54] Our results also confirmed that SrBGM significantly enhanced the M2 phenotype formation and PDGF-BB factor expression of macrophage (RAW cells) after 3 days incubation (Fig.3).

The possible mechanism of promoting early angiogenesis for SrBGM is illustrated in Fig. S6. After SrBGM was implanted under the skull subcutaneous, Si, Ca, P and Sr ions are quickly released from SrBGM. The Si, Ca and P ions have the effect to directly stimulate angiogenesis. Meanwhile, Sr will regulate macrophage phenotypes by promoting M1 to M2. Then, the M2 macrophages express high level PDGF-BB to promote the stabilize formation of vasculature. Due to the excellent early angiogenesis ability

of SrBGM *in vitro* and *in vivo*, the significantly improved bone regeneration *in vivo* was observed. In addition to the early angiogenesis effect on the osteogenesis, the Sr ions and other ions in SrBGM also have the ability to stimulate bone formation [55]. The osteogenesis-promoted effects of Si, Ca and P ions released from BG have been widely accepted as BG could stimulate the differentiation of osteoblasts and activate osteogenesis-related signaling pathways.[3] In addition, Sr is also reported to be able to enhance mineralization [56] and osteogenesis [10]. For example, Autefage *et al.* reported that SrBG enhanced the BMP2 gene expression of hMSC [57]. Moreover, a recent study indicated that the local release of Sr from Ti implants could improve early osseointegration [58]. Our previous research also confirms that Sr ions and other ions in Sr added BGM might synergistically mediate the enhanced osteogenesis by Sr activating NFATc signaling pathway and silicate activating Wnt/ β -catenin signaling pathway [59]. Although here we showed the bone regeneration potential using SrBGM through enhancing early angiogenesis by regulating the macrophage phenotype, SrBGM was probably also useful for other tissue repair and regeneration. Further studies should be carried out to investigate the molecular mechanism of macrophage phenotype regulation by SrBGM and demonstrate their applications in soft tissue regeneration such as muscle and skin.

4. Conclusions

In summary, SrBGM has no significant difference effect on the angiogenesis of HUVECs compared with BGM. SrBGM can regulate macrophage (RAW cells) phenotypes by promoting M1 to M2 and express high level of PDGF-BB which contributes to the angiogenesis. In addition, SrBGM+RAW conditioned medium significantly enhance the angiogenesis ability of HUVECs. *In vivo* experiments further confirmed that SrBGM can promote early vascularization and induce macrophage to polarize M2 phenotype at the

implantation site in a bone augmentation model. This study demonstrates that SrBGM could enhance the early angiogenesis through immune regulation effect and have wide application in ischemic tissue regeneration.

Acknowledgements

This study was financially supported by the National Natural Science Foundation of China (grant no. 51672088, 51502237, 31430030, 81501861), the Joint Funds of the National Natural Science Foundation of China (grant no. U1501245), the Beijing Municipal Commission of Health and Family Planning (grant no. PXM2018_026275_000001) and the Natural Science Foundation of Guangdong Province (grant no. 2015A030310034).

Data availability statement

The raw/processed data required to reproduce these findings cannot be shared at this time as the data also forms part of an ongoing study.

References

- [1] C. Mertens, O. Thiele, M. Engel, R. Seeberger, J. Hoffmann, K. Freier, The Use of Self-Inflating Soft Tissue Expanders Prior to Bone Augmentation of Atrophied Alveolar Ridges, *Clin Implant Dent R* 17(1) (2015) 44-51.
- [2] Y. Xue, Y. Guo, M. Yu, M. Wang, P. X. Ma, B. Lei, Monodispersed Bioactive Glass Nanoclusters with Ultralarge Pores and Intrinsic Exceptionally High miRNA Loading for Efficiently Enhancing Bone Regeneration, *Adv. Healthcare Mater.* (2017) 1700630.
- [3] J.R. Jones, Review of bioactive glass: from Hench to hybrids, *Acta Biomater.* 9(1) (2013) 4457-4486.
- [4] R. Margonar, T.P. Queiroz, E.R. Luvizuto, E. Marcantonio, R.C.C. Lia, M. Holzhausen, E.

Marcantonio-Junior, Bioactive glass for alveolar ridge augmentation, *J. Craniofac. Surg.* 23(3) (2012) 220-222.

[5] O.-M. Goudouri, E. Kontonasaki, K. Chrissafis, K. Zinn, A. Hoppe, R. Detsch, K.M. Paraskevopoulos, A.R. Boccaccini, Towards the synthesis of an Mg-containing silicate glass–ceramic to be used as a scaffold for cementum/alveolar bone regeneration, *Ceram. Int.* 40(10) (2014) 16287-16298.

[6] F Li, M. Wang, G. Pi, B. Lei, Europium Doped Monodispersed Bioactive Glass Nanoparticles Regulate the Osteogenic Differentiation of Human Marrow Mesenchymal Stem Cells, *J. Biomed. Nanotechnol.* 14(2018) 756-764.

[7] A. Hoppe, N.S. Gldal, A.R. Boccaccini, A review of the biological response to ionic dissolution products from bioactive glasses and glass-ceramics, *Biomaterials* 32(11) (2011) 2757-2774.

[8] I. Cacciotti, Bivalent cationic ions doped bioactive glasses: the influence of magnesium, zinc, strontium and copper on the physical and biological properties, *J. Mater. Sci.* 52(15) (2017) 8812-8831.

[9] C. Wu, J. Chang, Multifunctional mesoporous bioactive glasses for effective delivery of therapeutic ions and drug/growth factors, *J. Control. Release* 193 (2014) 282-295.

[10] M. Pilmane, K. Salma-Ancane, D. Loca, J. Locs, L. Berzina-Cimdina, Strontium and strontium ranelate: Historical review of some of their functions, *Mater. Sci. Eng. C* 78 (2017) 1222-1230.

[11] J. Shi, Y. Li, Y. Gu, S. Qiao, X. Zhang, H. Lai, Effect of titanium implants with strontium incorporation on bone apposition in animal models: A systematic review and meta-analysis, *Sci. Rep.* 7(1) (2017) 15563.

[12] K. Lin, L. Xia, H. Li, X. Jiang, H. Pan, Y. Xu, W.W. Lu, Z. Zhang, J. Chang, Enhanced osteoporotic bone regeneration by strontium-substituted calcium silicate bioactive ceramics, *Biomaterials* 34(38) (2013) 10028-10042.

- [13] F. Yang, D. Yang, J. Tu, Q. Zheng, L. Cai, L. Wang, Strontium Enhances Osteogenic Differentiation of Mesenchymal Stem Cells and In Vivo Bone Formation by Activating Wnt/Catenin Signaling, *Stem Cells* 29(6) (2011) 981-991.
- [14] O. Fromigue, E. Hay, A. Barbara, C. Petrel, E. Traiffort, M. Ruat, P.J. Marie, Calcium sensing receptor-dependent and receptor-independent activation of osteoblast replication and survival by strontium ranelate, *J. Cell. Mol. Med.* 13(8B) (2009) 2189-2199.
- [15] S. Tenti, S. Cheleschi, G.M. Guidelli, M. Galeazzi, A. Fioravanti, What about strontium ranelate in osteoarthritis? Doubts and securities, *Mod. Rheumatol.* 24(6) (2014) 881-884.
- [16] J. Zarins, M. Pilmane, E. Sidhoma, I. Salma, Does Local Application of Strontium Increase Osteogenesis and Biomaterial Osteointegration in Osteoporotic and Other Bone Tissue Conditions: Review of Literature, *Acta Chirurgica Latviensis* 16(2) (2016) 17-23.
- [17] X. Wang, Y. Wang, L. Li, Z. Gu, H. Xie, X. Yu, Stimulation of strontium-doped calcium polyphosphate for bone tissue engineering to protein secretion and mRNA expression of the angiogenic growth factors from endothelial cells in vitro, *Ceram. Int.* 40(5) (2014) 6999-7005.
- [18] S. Zhao, J. Zhang, M. Zhu, Y. Zhang, Z. Liu, C. Tao, Y. Zhu, C. Zhang, Three-dimensional printed strontium-containing mesoporous bioactive glass scaffolds for repairing rat critical-sized calvarial defects, *Acta Biomater.* 12(15) (2015) 270-280.
- [19] Z. Gu, H. Xie, L. Li, X. Zhang, F. Liu, X. Yu, Application of strontium-doped calcium polyphosphate scaffold on angiogenesis for bone tissue engineering, *J. Mater. Sci. Mater. Med.* 24(5) (2013) 1251-1260.
- [20] L. Mao, L. Xia, J. Chang, J. Liu, L. Jiang, C. Wu, B. Fang, The synergistic effects of Sr and Si bioactive ions on osteogenesis, osteoclastogenesis and angiogenesis for osteoporotic bone regeneration, *Acta Biomater.*

61 (2017) 217-232.

[21] W. Zhang, H. Cao, X. Zhang, G. Li, Q. Chang, J. Zhao, Y. Qiao, X. Ding, G. Yang, X. Liu, X. Jiang, A strontium-incorporated nanoporous titanium implant surface for rapid osseointegration, *Nanoscale* 8(9) (2016) 5291-5301.

[22] Z. Chen, T. Klein, R.Z. Murray, R. Crawford, J. Chang, C. Wu, Y. Xiao, Osteoimmunomodulation for the development of advanced bone biomaterials, *Mater. Today* 19(6) (2016) 304-321.

[23] K.L. Spiller, T.J. Koh, Macrophage-based therapeutic strategies in regenerative medicine, *Adv. Drug Del. Rev.* 122 (2017) 74-83.

[24] D.M. Mosser, J.P. Edwards, Exploring the full spectrum of macrophage activation, *Nature Reviews Immunology* 8(12) (2008) 958-969.

[25] S. Franz, S. Rammelt, D. Scharnweber, J.C. Simon, Immune responses to implants - A review of the implications for the design of immunomodulatory biomaterials, *Biomaterials* 32(28) (2011) 6692-6709.

[26] C.N. Serhan, N. Chiang, J. Dalli, The resolution code of acute inflammation: Novel pro-resolving lipid mediators in resolution, *Semin. Immunol.* 27(3) (2015) 200-215.

[27] J.D. Roh, R. Sawh-Martinez, M.P. Brennan, S.M. Jay, L. Devine, D.A. Rao, T. Yi, T.L. Mirensky, A. Nalbandian, B. Udelsman, N. Hibino, T. Shinoka, W.M. Saltzman, E. Snyder, T.R. Kyriakides, J.S. Pober, C.K. Breuer, Tissue-engineered vascular grafts transform into mature blood vessels via an inflammation-mediated process of vascular remodeling, *Proceedings of the National Academy of Sciences* 107(10) (2010) 4669-4674.

[28] N. Hibino, T. Yi, D.R. Duncan, A. Rathore, E. Dean, Y. Naito, A. Dardik, T. Kyriakides, J. Madri, J.S. Pober, T. Shinoka, C.K. Breuer, A critical role for macrophages in neovessel formation and the development

of stenosis in tissue-engineered vascular grafts, *FASEB J.* 25(12) (2011) 4253-4263.

[29] J. Ng, K. Spiller, J. Bernhard, G. Vunjak-Novakovic, Biomimetic Approaches for Bone Tissue Engineering, *Tissue Engineering Part B: Reviews* 23(5) (2016) 480-493.

[30] N. Jetten, S. Verbruggen, M.J. Gijbels, M.J. Post, M.P.J. De Winther, M.M.P.C. Donners, Anti-inflammatory M2, but not pro-inflammatory M1 macrophages promote angiogenesis in vivo, *Angiogenesis* 17(1) (2014) 109-118.

[31] E. Zajac, B. Schweighofer, T.A. Kupriyanova, A. Juncker-Jensen, P. Minder, J.P. Quigley, E.I. Deryugina, Angiogenic capacity of M1-and M2-polarized macrophages is determined by the levels of TIMP-1 complexed with their secreted proMMP-9, *Blood* 122(25) (2013) 4054-4067.

[32] B.N. Brown, R. Londono, S. Tottey, L. Zhang, K.A. Kukla, M.T. Wolf, K.A. Daly, J.E. Reing, S.F. Badylak, Macrophage phenotype as a predictor of constructive remodeling following the implantation of biologically derived surgical mesh materials, *Acta Biomater.* 8(3) (2012) 978-987.

[33] C. Troidl, G. Jung, K. Troidl, J. Hoffmann, H. Mollmann, H. Nef, W. Schaper, C.W. Hamm, T. Schmitz-Rixen, The Temporal and Spatial Distribution of Macrophage Subpopulations During Arteriogenesis, *Curr. Vasc. Pharmacol.* 11(1) (2013) 5-12.

[34] M. Moises Alvarez, J.C. Liu, G. Trujillo-de Santiago, B.-H. Cha, A. Vishwakarma, A.M. Ghaemmaghami, A. Khademhosseini, Delivery strategies to control inflammatory response: Modulating M1-M2 polarization in tissue engineering applications, *J. Control. Release* 240 (2016) 349-363.

[35] Z. Julier, A.J. Park, P.S. Briquez, M.M. Martino, Promoting tissue regeneration by modulating the immune system, *Acta Biomater.* 53 (2017) 13-28.

[36] Y. Xue, Y. Du, J. Yan, Z. Liu, P. X. Ma, X. Chen, B. Lei, Monodisperse photoluminescent and highly

biocompatible bioactive glass nanoparticles for controlled drug delivery and cell imaging, *J. Mater. Chem. B* 3(18) (2015) 3831-3839.

[37] W. Zhang, F. Zhao, D. Huang, X. Fu, X. Li, X. Chen, Strontium-Substituted Submicrometer Bioactive Glasses Modulate Macrophage Responses for Improved Bone Regeneration, *ACS Applied Materials & Interfaces* 8(45) (2016) 30747-30758.

[38] L.A. Kinard, R.L. Dahlin, J. Lam, S. Lu, E.J. Lee, F.K. Kasper, A.G. Mikos, Synthetic biodegradable hydrogel delivery of demineralized bone matrix for bone augmentation in a rat model, *Acta Biomater.* 10(11) (2014) 4574-4582.

[39] C.M. Champagne, J. Takebe, S. Offenbacher, L.F. Cooper, Macrophage cell lines produce osteoinductive signals that include bone morphogenetic protein-2, *Bone* 30(1) (2002) 26-31.

[40] D.O. Freytes, J.W. Kang, I. Marcos-Campos, G. Vunjak-Novakovic, Macrophages modulate the viability and growth of human mesenchymal stem cells, *J Cell Biochem* 114(1) (2013) 220-229.

[41] F. Loi, L.A. Cordova, J. Pajarinen, T.-h. Lin, Z. Yao, S.B. Goodman, Inflammation, fracture and bone repair, *Bone* 86 (2016) 119-130.

[42] A.A. Gorustovich, J.A. Roether, A.R. Boccaccini, Effect of bioactive glasses on angiogenesis: a review of in vitro and in vivo evidences, *Tissue Engineering Part B: Reviews* 16(2) (2009) 199-207.

[43] S. Kargozar, F. Baino, S. Hamzehlou, R.G. Hill, M. Mozafari, Bioactive Glasses: Sprouting Angiogenesis in Tissue Engineering, *Trends Biotechnol.* 36(4) (2018) 430-444.

[44] Y. Zhou, M. Shi, J.R. Jones, Z. Chen, J. Chang, C. Wu, Y. Xiao, Strategies to direct vascularisation using mesoporous bioactive glass-based biomaterials for bone regeneration, *Int. Mater. Rev.* 62(7) (2017) 392-414.

[45] S. Li, L. Li, C. Guo, H. Qin, X. Yu, A promising wound dressing material with excellent

cytocompatibility and proangiogenesis action for wound healing: Strontium loaded Silk fibroin/Sodium alginate (SF/SA) blend films, *Int. J. Biol. Macromol.* 104 (2017) 969-978.

[46] S. Kargozar, N. Lotfibakhshaiesh, J. Ai, M. Mozafari, P. Brouki Milan, S. Hamzehlou, M. Barati, F. Baino, R.G. Hill, M.T. Joghataei, Strontium- and cobalt-substituted bioactive glasses seeded with human umbilical cord perivascular cells to promote bone regeneration via enhanced osteogenic and angiogenic activities, *Acta Biomater.* 58 (2017) 502-514.

[47] L. Weng, S.K. Boda, M.J. Teusink, F.D. Shuler, X. Li, J. Xie, Binary Doping of Strontium and Copper Enhancing Osteogenesis and Angiogenesis of Bioactive Glass Nanofibers while Suppressing Osteoclast Activity, *ACS Applied Materials & Interfaces* 9(29) (2017) 24484-24496.

[48] E. Buache, F. Velard, E. Bauden, C. Guillaume, E. Jallot, J.M. Nedelec, D. Laurent-Maquin, P. Laquerriere, Effect of strontium-substituted biphasic calcium phosphate on inflammatory mediators production by human monocytes, *Acta Biomater.* 8(8) (2012) 3113-3119.

[49] C.-H. Lee, Y.-J. Kim, J.-H. Jang, J.-W. Park, Modulating macrophage polarization with divalent cations in nanostructured titanium implant surfaces, *Nanotechnology* 27(8) (2016) 085101.

[50] C. Cardemil, I. Elgali, W. Xia, L. Emanuelsson, B. Norlindh, O. Omar, P. Thomsen, Strontium-Doped Calcium Phosphate and Hydroxyapatite Granules Promote Different Inflammatory and Bone Remodelling Responses in Normal and Ovariectomised Rats, *PLoS One* 8(12) (2013) e84932.

[51] X. Dong, J. Chang, H. Li, Bioglass promotes wound healing through modulating the paracrine effects between macrophages and repairing cells, *J. Mater. Chem. B* 5(26) (2017) 5240-5250.

[52] J. Wang, S. Qian, X. Liu, L. Xu, X. Miao, Z. Xu, L. Cao, H. Wang, X. Jiang, M2 macrophages contribute to osteogenesis and angiogenesis on nanotubular TiO₂ surfaces, *J. Mater. Chem. B* 5(18) (2017) 3364-3376.

- [53] K.L. Spiller, S. Nassiri, C.E. Witherel, R.R. Anfang, J. Ng, K.R. Nakazawa, T. Yu, G. Vunjak-Novakovic, Sequential delivery of immunomodulatory cytokines to facilitate the M1-to-M2 transition of macrophages and enhance vascularization of bone scaffolds, *Biomaterials* 37 (2015) 194-207.
- [54] S.G. Ball, C.A. Shuttleworth, C.M. Kielty, Platelet-derived growth factor receptors regulate mesenchymal stem cell fate: implications for neovascularization, *Expert Opin. Biol. Ther.* 10(1) (2010) 57-71.
- [55] Y. Du, M. Yu, J. Ge, P. X. Ma, X. Chen, B. Lei, Development of a Multifunctional Platform Based on Strong, Intrinsically Photoluminescent and Antimicrobial Silica□Poly (citrate)s□Based Hybrid Biodegradable Elastomers for Bone Regeneration, *Adv. Funct. Mater.* 31(25) (2015) 5016-5029.
- [56] G. Molino, A. Bari, F. Baino, S. Fiorilli, C. Vitale-Brovarone, Electrophoretic deposition of spray-dried Sr-containing mesoporous bioactive glass spheres on glass-ceramic scaffolds for bone tissue regeneration, *J. Mater. Sci.* 52(15) (2017) 9103-9114.
- [57] H. Autefage, E. Gentleman, E. Littmann, M.A.B. Hedegaard, T. Von Erlach, M. O'Donnell, F.R. Burden, D.A. Winkler, M.M. Stevens, Sparse feature selection methods identify unexpected global cellular response to strontium-containing materials, *Proc. Natl. Acad. Sci. U. S. A.* 112(14) (2015) 4280-4285.
- [58] V. Offermanns, O.Z. Andersen, G. Riede, M. Sillassen, C.S. Jeppesen, K.P. Almqvist, H. Talasz, C. Öhman-Mägi, B. Lethaus, R. Tolba, F. Kloss, M. Foss, Effect of strontium surface-functionalized implants on early and late osseointegration: A histological, spectrometric and tomographic evaluation, *Acta Biomater.* 69 (2018) 385-394.
- [59] W. Zhang, D. Huang, F. Zhao, W. Gao, L. Sun, X. Li, X. Chen, Synergistic effect of strontium and silicon in strontium-substituted sub-micron bioactive glass for enhanced osteogenesis, *Mater. Sci. Eng. C* 89 (2018)

245-255.

ACCEPTED MANUSCRIPT

Figure captions

Fig. 1 Physicochemical structure characterizations of SrBGM and SrBGM-based scaffolds. (A) SEM images and EDS spectra of BGM and SrBGM; (B) XRD spectra and (C) FTIR spectra of BGM and SrBGM; (D) SEM images of Gel, Gel-BGM and Gel-SrBGM scaffolds, the second line was enlarged position of white squares in first line, the insert images in first line was Micro-CT images of the scaffolds.

Fig. 2 *In vitro* angiogenesis evaluations of HUVECs stimulated by the extracts of BGM and SrBGM, tissue culture plate and SrCl₂ were used as controls. (A) Immunostaining images of CD31 (red) and DAPI (blue); (B) Quantification of the immunostaining intensity of CD31; (C) mRNA expression of angiogenesis-related genes (Angiogenin, FGF-2 and SDF) of HUVECs cultured for 3 days. Notes: * $p < 0.05$ compared to Control; # $p < 0.05$ compared to BGM.

Fig. 3 Macrophage polarization and promoting angiogenesis potential after cultured with Control, BGM, SrBGM and SrCl₂ for 3 days. (A) Flow cytometry results of RAW (CD11c is a marker for M1; CD206 is a marker for M2); (B) mRNA expression of inflammation-related genes TNF α , IL1 β , IL6, IL1ra, IL10 and Arginase; (C) mRNA expression of angiogenesis-related genes VEGF and PDGF-BB; (D) western blot analysis of PDGF-BB protein; (E) quantitative analysis of relative protein levels of PDGF-BB at different groups. Notes: * $p < 0.05$ compared to Control; # $p < 0.05$ compared to BGM.

Fig. 4 Angiogenesis of HUVECs under RAW conditioned medium for 3 days. (A) Immunostaining images of CD31 (red) and DAPI (blue), the yellow arrows indicates circles position; (B) Quantification of the immunostaining intensity of CD31; (C) mRNA expression of angiogenesis-related genes (Angiogenin, FGF-2 and SDF) of HUVECs cultured for 3 days. Notes: * $p < 0.05$ compared to Control+RAW; # $p < 0.05$ compared to BGM+RAW.

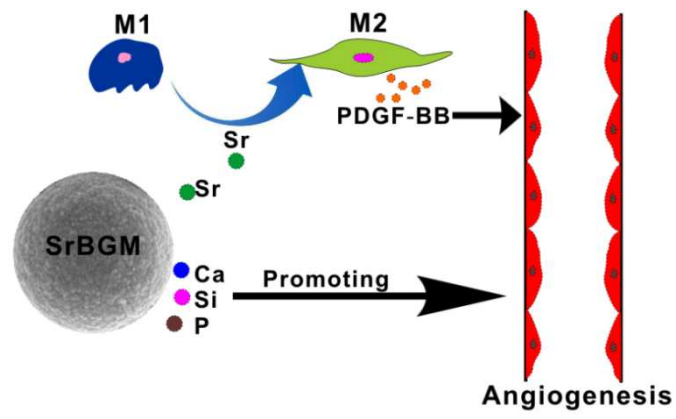
Fig. 5 Evaluation of *in vivo* angiogenesis after implantation for 1 week. (A) Gross observation of Gel, Gel-BGM and Gel-SrBGM scaffolds together with surrounding tissue; (B) 3D reconstruction images of the scaffolds and surrounding tissue by Micro-CT analysis; (C) H&E histological images of the scaffolds with around tissues: the first line was general view of longitudinal section; the second line was the magnification of the center area of the scaffolds (yellow box in first column); (D) CD31 immunohistochemical staining of the similar position with H&E. The yellow arrows represents vascular-like structures; the red arrows represents the CD31 stained positive staining.

Fig. 6 Immunohistochemical evaluation of macrophage polarization in Gel, Gel-BGM and Gel-SrBGM scaffolds after implantation *in vivo* for 1 week. NOS2 was a marker of M1 macrophage. CD206 and Arginase I were markers of M2 macrophage.

Fig. 7 *In vivo* bone regeneration evaluation of Gel, Gel-BGM and Gel-SrBGM scaffolds at 6 weeks. (A) Gross observation of scaffolds and surrounding tissue; (B) 3D reconstruction images of scaffolds and surrounding tissue by Micro-CT; (C) Morphometric analysis of the bone volume to total volume (BV/TV) based on the Micro-CT results; (D) Masson's trichrome staining images of the scaffolds with around tissues: the first line was general view of longitudinal section; the second line was the magnification of the center area of the scaffolds (yellow box in first column). Symbols were residual scaffolds (RS), new bone (NB) and osteoblasts (yellow arrows) * indicates a significant difference, $p < 0.05$.

Fig. 8 Schematic illustration of SrBGM promoting angiogenesis mechanism. The Si, Ca and P ion have the effect to directly stimulation angiogenesis. Sr will regulate macrophage phenotypes by promoting M1 to M2. Then, the M2 express PDGF-BB promoting the stabilize formation of vasculature.

Graphic Abstract



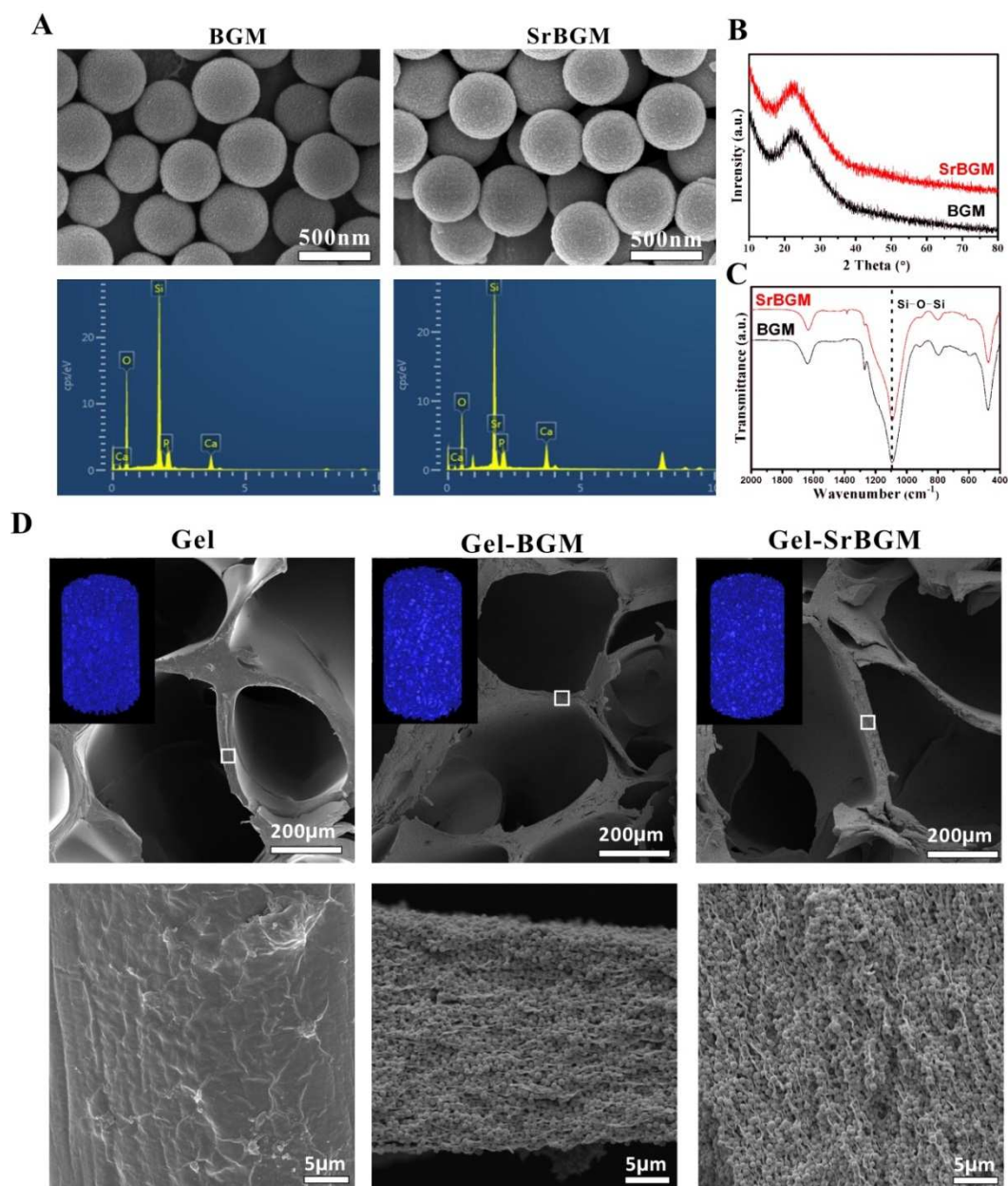


Fig. 1 Physicochemical structure characterizations of SrBGM and SrBGM-based scaffolds. (A) SEM images and EDS spectra of BGM and SrBGM; **(B)** XRD spectra and **(C)** FTIR spectra of BGM and SrBGM; **(D)** SEM images of Gel, Gel-BGM and Gel-SrBGM scaffolds, the second line was enlarged position of white squares in first line, the insert images in first line was Micro-CT images of the scaffolds.

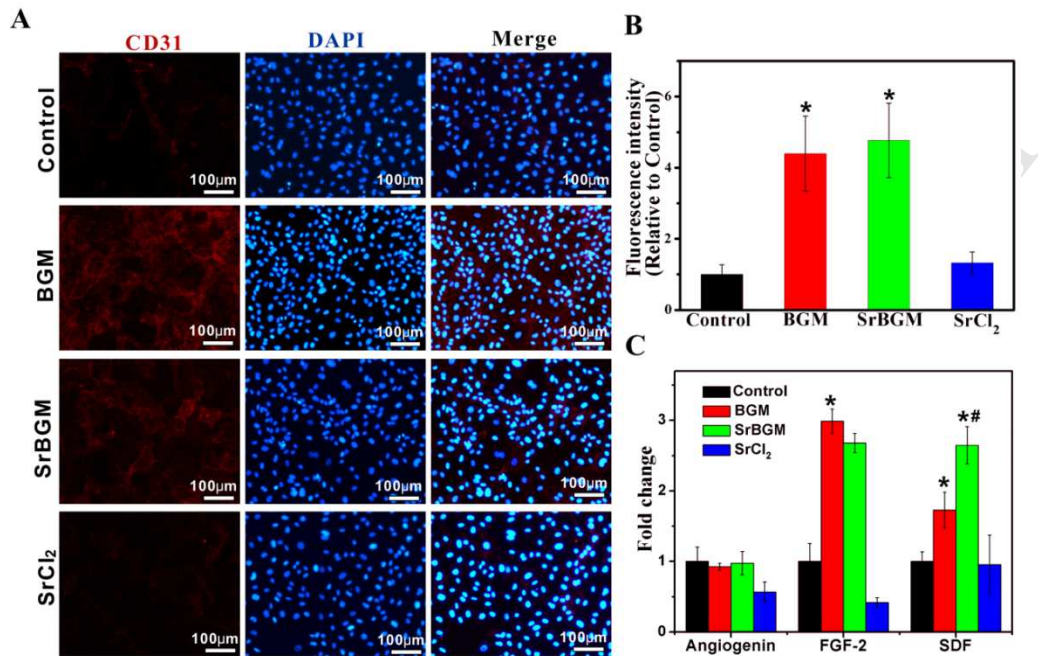


Fig. 2 *In vitro* angiogenesis evaluations of HUVECs stimulated by the extracts of BGM and SrBGM, tissue culture plate and SrCl₂ were used as controls. (A) Immunostaining images of CD31 (red) and DAPI (blue); (B) Quantification of the immunostaining intensity of CD31; (C) mRNA expression of angiogenesis-related genes (Angiogenin, FGF-2 and SDF) of HUVECs cultured for 3 days. Notes: * $p < 0.05$ compared to Control; # $p < 0.05$ compared to BGM.

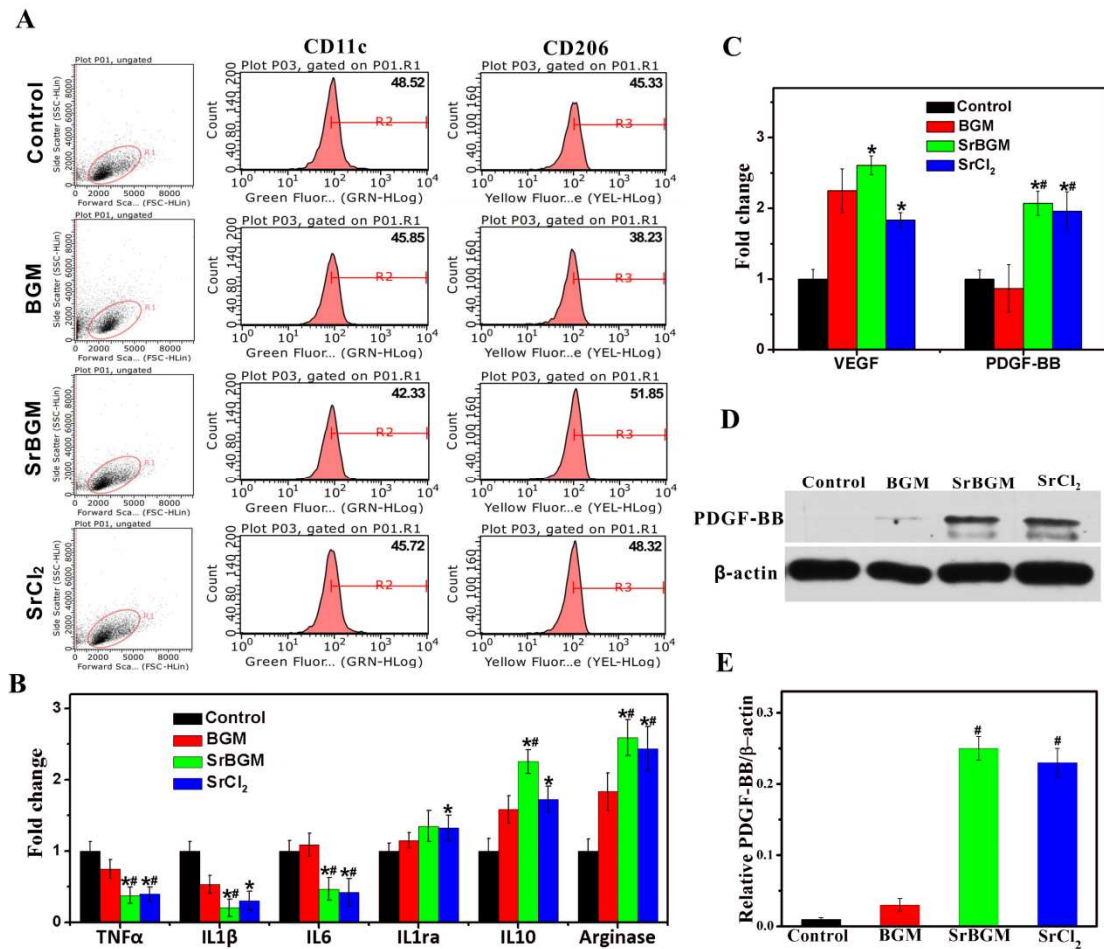


Fig. 3 Macrophage polarization and promoting angiogenesis potential after cultured with Control, BGM, SrBGM and SrCl₂ for 3 days. (A) Flow cytometry results of RAW (CD11c is a marker for M1; CD206 is a marker for M2); (B) mRNA expression of inflammation-related genes TNF α , IL1 β , IL6, IL1ra, IL10 and Arginase; (C) mRNA expression of angiogenesis-related genes VEGF and PDGF-BB; (D) western blot analysis of PDGF-BB protein; (E) quantitative analysis of relative protein levels of PDGF-BB at different groups. Notes: * $p < 0.05$ compared to Control; # $p < 0.05$ compared to BGM.

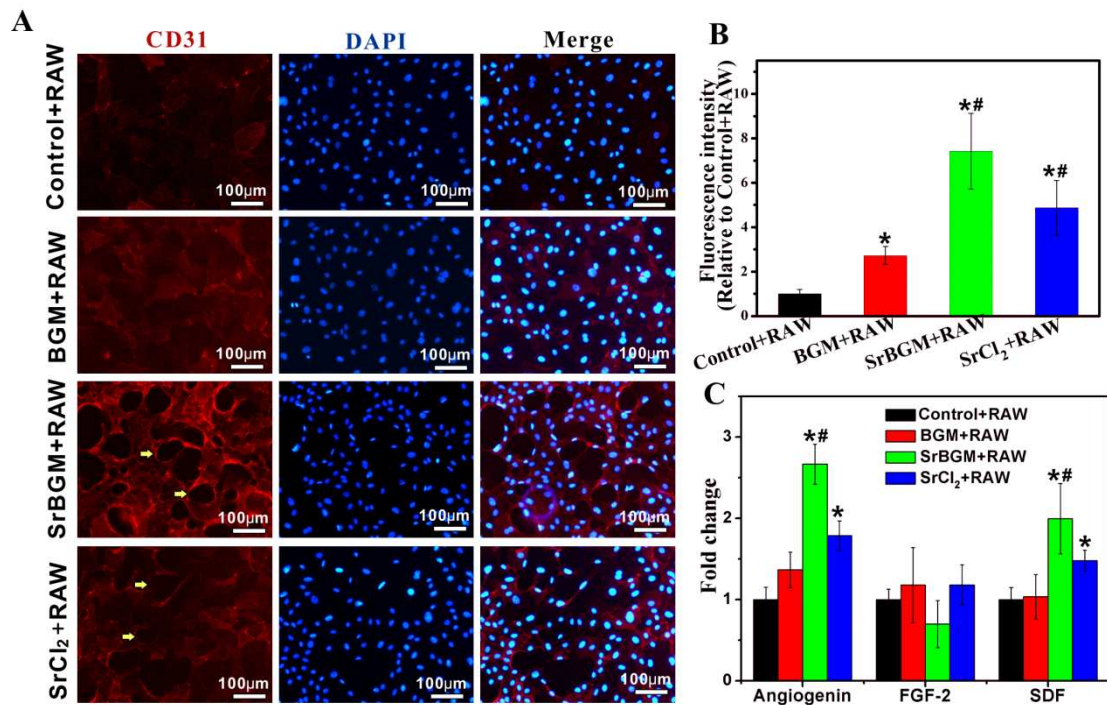


Fig. 4 Angiogenesis of HUVECs under RAW conditioned medium for 3 days. (A) Immunostaining images of CD31 (red) and DAPI (blue), the yellow arrows indicates circles position; (B) Quantification of the immunostaining intensity of CD31; (C) mRNA expression of angiogenesis-related genes (Angiogenin, FGF-2 and SDF) of HUVECs cultured for 3 days. Notes: * $p < 0.05$ compared to Control+RAW; # $p < 0.05$ compared to BGM+RAW.

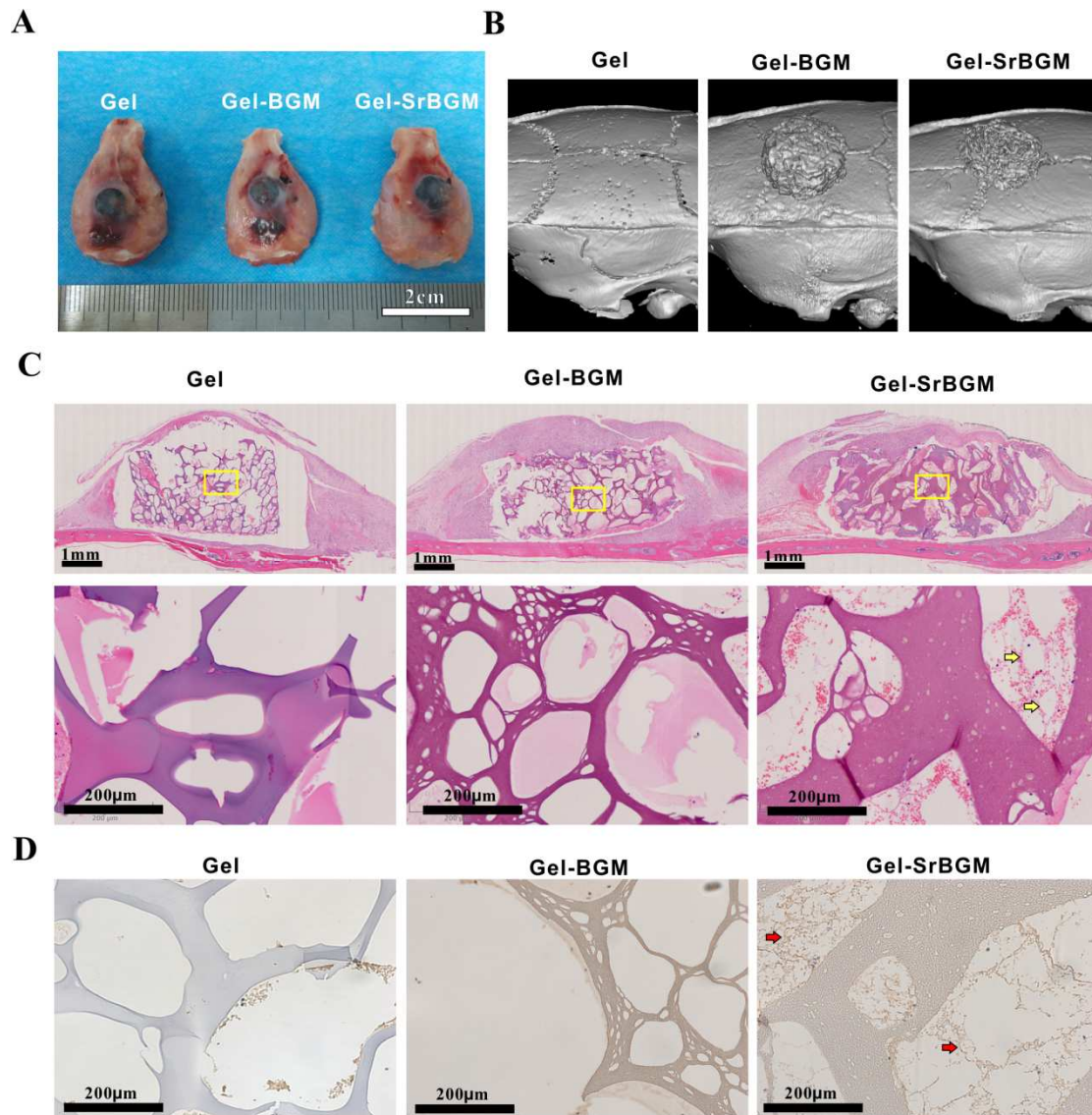


Fig. 5 Evaluation of *in vivo* angiogenesis after implantation for 1 week. (A) Gross observation of Gel, Gel-BGM and Gel-SrBGM scaffolds together with surrounding tissue; (B) 3D reconstruction images of the scaffolds and surrounding tissue by Micro-CT analysis; (C) H&E histological images of the scaffolds with around tissues: the first line was general view of longitudinal section; the second line was the magnification of the center area of the scaffolds (yellow box in first column); (D) CD31 immunohistochemical staining of the similar position with H&E. The yellow arrows represents vascular-like structures; the red arrows represents the CD31 stained positive staining.

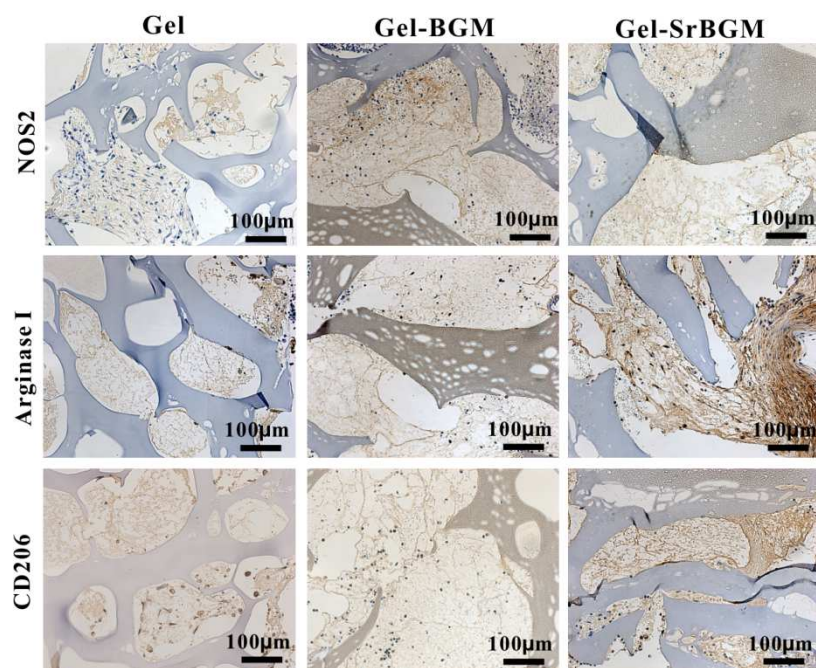


Fig. 6 Immunohistochemical evaluation of macrophage polarization in Gel, Gel-BGM and Gel-SrBGM scaffolds after implantation *in vivo* for 1 week. NOS2 was a marker of M1 macrophage. CD206 and Arginase I were markers of M2 macrophage.

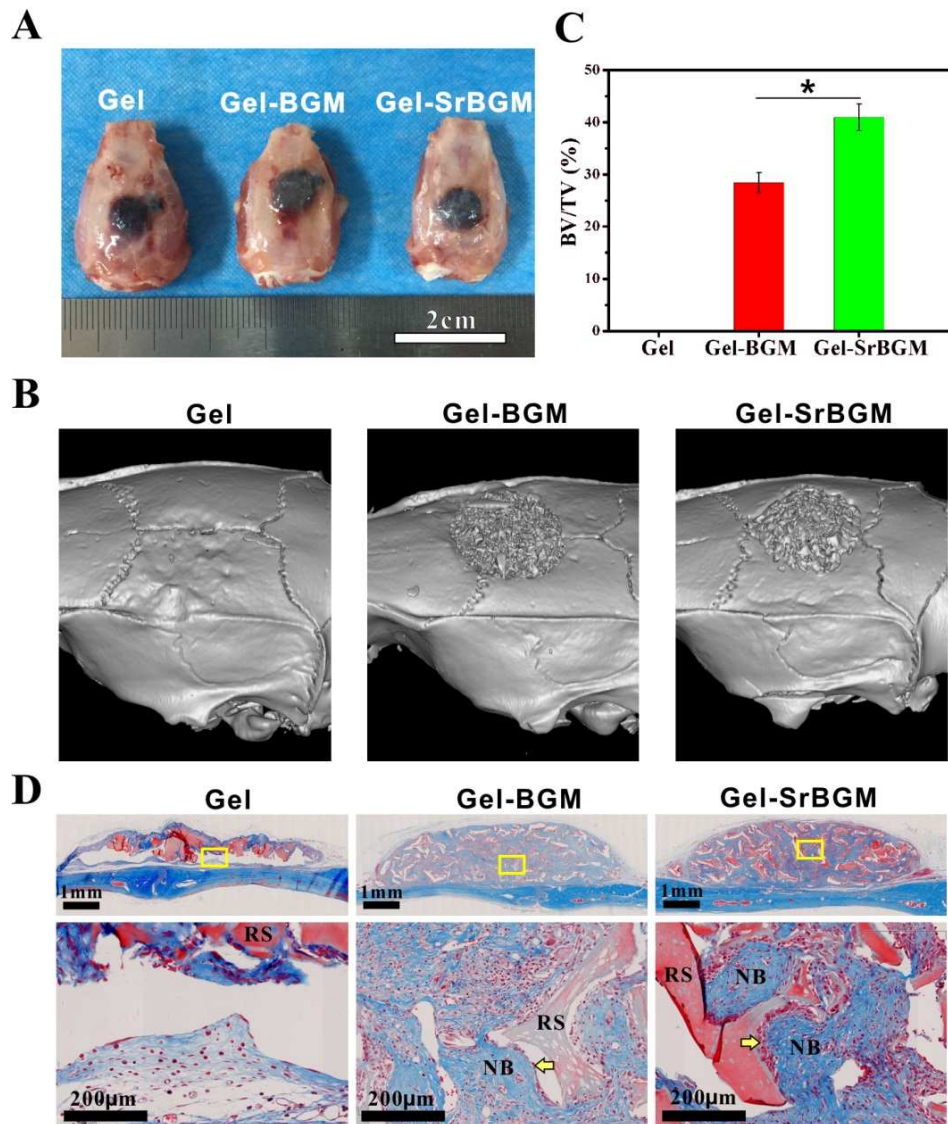


Fig. 7 *In vivo* bone regeneration evaluation of Gel, Gel-BGM and Gel-SrBGM scaffolds at 6 weeks.

(A) Gross observation of scaffolds and surrounding tissue; (B) 3D reconstruction images of scaffolds and surrounding tissue by Micro-CT; (C) Morphometric analysis of the bone volume to total volume (BV/TV) based on the Micro-CT results; (D) Masson's trichrome staining images of the scaffolds with around tissues: the first line was general view of longitudinal section; the second line was the magnification of the center area of the scaffolds (yellow box in first column). Symbols were residual scaffolds (RS), new bone (NB) and osteoblasts (yellow arrows) * indicates a significant difference, $p < 0.05$.